


RESEARCH ARTICLE

Open Access

Use of quantitative T2 mapping for the assessment of renal cell carcinomas: first results



Lisa C. Adams^{1*} , Keno K. Bressemer², Phillipp Jurmeister³, Ute L. Fahlenkamp¹, Bernhard Ralla⁴, Guenther Engel¹, Bernd Hamm¹, Jonas Busch¹ and Marcus R. Makowski¹

Abstract

Background: Correct staging and grading of patients with clear cell renal cell carcinoma (cRCC) is of clinical relevance for the prediction of operability and for individualized patient management. As partial or radial resection with postoperative tumor grading currently remain the methods of choice for the classification of cRCC, non-invasive preoperative alternatives to differentiate lower grade from higher grade cRCC would be beneficial.

Methods: This institutional-review-board approved cross-sectional study included twenty-seven patients (8 women, mean age \pm SD, 61.3 ± 14.2) with histopathologically confirmed cRCC, graded according to the International Society of Urological Pathology (ISUP). A native, balanced steady-state free precession T2 mapping sequence (TrueFISP) was performed at 1.5 T. Quantitative T2 values were measured with circular 2D ROIs in the solid tumor portion and also in the normal renal parenchyma (cortex and medulla). To estimate the optimal cut-off T2 value for identifying lower grade cRCC, a Receiver Operating Characteristic Curve (ROC) analysis was performed and sensitivity and specificity were calculated. Students' t-tests were used to evaluate the differences in mean values for continuous variables, while intergroup differences were tested for significance with two-tailed Mann-Whitney-U tests.

Results: There were significant differences between the T2 values for lower grade (ISUP 1–2) and higher grade (ISUP 3–4) cRCC ($p < 0.001$), with higher T2 values for lower grade cRCC compared to higher grade cRCC. The sensitivity and specificity for the differentiation of lower grade from higher grade tumors were 83.3% (95% CI: 0.59–0.96) and 88.9% (95% CI: 0.52–1.00), respectively, using a threshold value of ≥ 110 ms. Intraobserver/interobserver agreement for T2 measurements was excellent/substantial.

Conclusions: Native T2 mapping based on a balanced steady-state free precession MR sequence might support an image-based distinction between lower and higher grade cRCC in a two-tier-system and could be a helpful addition to multiparametric imaging.

Keywords: MRI mapping techniques, Quantitative MRI, T2 mapping, Clear cell renal cell carcinoma, Tumor grading

Background

Globally, renal cell carcinomas (RCC) have significant impact with approximately 65,000 new cases in the United States and 84,000 cases in the European Union each year [1, 2], with clear cell renal cell carcinomas (cRCC) being the most common subtype [3, 4]. Given that lower grade cRCC carry a significantly better prognosis than higher grade cRCC, it would be desirable to

individualize treatment options, which could entail a radical approach for higher grade cRCC and a more conservative management such as active surveillance for lower grade cRCC [5]. Currently, partial or radial resection with postoperative tumor grading remains the method of choice for the classification of cRCC, because image-based biopsies or fine needle aspiration remain controversial due to their invasiveness, sampling errors, and risk of needle tract seeding [6]. Therefore, non-invasive preoperative alternatives to differentiate lower grade from higher grade cRCC would be beneficial [6].

* Correspondence: Lisa.adams@charite.de

¹Department of Radiology, Charité, Charitéplatz 1, 10117 Berlin, Germany
Full list of author information is available at the end of the article



Magnetic resonance imaging (MRI) is a non-invasive imaging modality, not relying on ionizing radiation. T2 weighted MRI sequences allow for visualization of inflammation and edema [7]. While conventional MRI only enables a qualitative image interpretation based on signal intensity analysis with arbitrary units, T2 mapping with voxel-wise evaluation of proton spin-spin relaxation times allows for a non-invasive visualization and quantification of tissue composition [8]. As quantitative T2 values reflect tissue composition and, in particular, free water content, T2 mapping is sensitive to tissue hydration or edema without the need for contrast agents and thus shows the potential to become a ‘non-invasive biopsy’ [9, 10].

While initially developed in the context of cardiac imaging, e.g. for quantification of myocardial edema as an early predictor of myocardial injury [7], T2-weighted parametric mapping techniques are increasingly applied in other organs, such as the liver or kidney, providing a pixel-by-pixel map of various T2 relaxation times [11–13].

In the context of brain tumors, it was previously suggested that tumors with higher cellularity showed a corresponding reduction in the extracellular fluid space [14]. While lower grade cRCC are associated with small nucleoli and low nuclear-to-cytoplasmic ratios, higher grade cRCC are characterized by nuclear polymorphism, higher cellularity and nuclear-to-cytoplasmic ratios [15], whereby it can be assumed that the extracellular fluid is subsequently decreased.

We hypothesized, that quantitative T2 mapping could be used to distinguish lower from higher grade cRCC by visualization of differences in tissue composition, e.g. extracellular liquid. This proof-of-concept study therefore investigates the feasibility of a T2 mapping approach to grade cRCC, correlating imaging findings with the corresponding histology.

Methods

Study population

This cross-sectional study was approved by the local Institutional Review board with written consent obtained from all participants prior to examinations. Between January 2017 and October 2018, 42 consecutive patients with suspected RCC, who agreed to participate, had no previous ablations or contraindications to MRI, were referred to our department for abdominal MRI. Out of these, 27 patients with histologically validated cRCC were included in the final analysis. The exclusions were as follows: 3 patients with urothelial carcinomas, 2 patients with oncocytomas, 2 patients with atypical angiomyolipomas, 2 patients without histologic examination (missing data on the reference standard), 4 patients with incorrect acquisition protocols and 2 patients with insufficient image quality due to motion artifacts.

Imaging protocol

Image acquisitions were performed using a 1.5 T clinical MRI scanner (Avanto; Siemens Medical Solutions, Erlangen, Germany) with dedicated 18-channel body and spine matrix coils. Apart from a clinical routine image protocol of the kidneys, the patients received a native, balanced steady-state free precession T2 mapping sequence (T2-prepared single-shot TrueFISP) in coronal plane, which was adjusted to the long axis of the kidney. The routine imaging protocol of the kidney included a coronal/sagittal T2 half Fourier single-shot turbo spin echo sequence (HASTE), a native coronal 3D gradient echo pulse T1-weighted (FLASH) sequence, a T1-FLASH angiography (contrast agent: gadoterate meglumine (Dotarem®, Guerbet, France), and a delayed fat saturated 3D T1 VIBE (volumetric interpolated breath-hold examination) sequence. Bolus tracking was used to determine the first pass and 3D FLASH images were obtained in the corticomedullary and nephrogenic phase. The T2-preparation was an iterative Carr-Purcell Malcom-Levitt (MLEV) sequence [16, 17]. T2 prepared-TrueFISP images were acquired at intervals of 3 interbeat/RR intervals with simulation of the electrocardiogram with 1 s per beat to allow for sufficient magnetization recovery in between acquisitions. For each image, the acquisition window was set in the same diastolic phase. The time of acquisition for the TrueFISP sequence was 14 s per slice acquisition, whereby T2 maps were acquired in three slices. All T2 maps were acquired prior to application of contrast agents. Please refer to Table 1 for detailed imaging parameters.

Table 1 Tabulated overview of MR imaging parameters

Sequence	T2-HASTE	True FISP*	T1 3D-FLASH*
Scan plane	Coronal	Coronal	Coronal
Voxel size (mm)	1.7 × 1.3 × 5.0	1.6 × 1.6 × 4.0	1.6 × 1.0 × 1.4
Number of slices	25	1	1
Slice thickness (mm)	5	4	1.40
TR/ TE (ms)	800/ 89	634.3/ 1.18	2.88/0.98
Averages	1	4	1
FoV (mm)	400	400	500
Flip angle (°)	170	70	25
Matrix	320	256	512
Bandwidth (Hz/Px)	422	930	440
Fat saturation	None	None	Yes
Parameter map type	–	T2 map (2D)	–
Number of T2 preps (lengths in ms)	–	3 (0; 24; 55)	–
Echo spacing (ms)	–	2.8	–
Phase encoding direction	R > > L	R > > L	R > > L

Descriptions: *FISP: Fast imaging with steady-state free precession.

**FLASH: Fast low-angle shot

T2 maps were automatically calculated on a pixel-by-pixel basis, based on the assumption of mono-exponential signal decay. They were displayed by a customized 12-bit lookup table with a visible colour map, whereby the signal intensity of each pixel reflected its absolute T2 value.

Imaging evaluation

PACS workstations (centricity radiology; GE Healthcare) were used for image evaluation/analysis. An evaluation of T2 mapping images was performed independently by two radiologists, who were blinded to the histopathological findings, enabling the assessment of interobserver agreement. One radiologist repeated the measurements after 2 weeks and two further ROI measurements were conducted after 3 months to enable a comprehensive intraobserver assessment. In large tumors with necrosis zones, circular 2D ROIs were placed within the most homogeneous and bright appearing portion of solid tumor area on the basis of visual assessment (in the postcontrast sequences), also in conjunction with T2-weighted images and were set in as large an area as possible. In small tumors without apparent necrosis zones, a circular 2D ROI was drawn around the entire tumor to avoid measurement inaccuracies (for illustration of exemplary measurements refer to Additional file 1: Figure S1). The respective ROIs were then copied to the TrueFISP (T2 mapping) sequence, using a semi-automatic co-registration tool. In case of breathing or motion artefacts, an additional visual correction was applied. As T2 maps were acquired within a single breath-hold, there was not motion between the different T2-weighted images. In all cases, it was taken care not to include the normal renal cortex, perinephric or sinus fat within the measured ROIs. Regions of necrosis and cystic degeneration were avoided and identified by lack of enhancement on postcontrast images [18, 19]. In one patient, who did not receive postcontrast imaging due to severe renal insufficiency, the initial 2D ROI was drawn in the T2 HASTE image in the most solid and homogeneous appearing tumor portion and then copied to the TrueFISP sequence. To measure the T2 values of renal cortex and medulla, 2D ROIs were placed in a healthy portion of the renal cortex and medulla, avoiding positioning on the boundary between cancerous and normal parenchyma. In case of extensive tumor infiltration of the kidney (which was the case in two patients), ROI measurements of the renal cortex and medulla were performed in the contralateral healthy kidney

ISUP grading

Resected cRCC specimens were examined by a pathologist. They were then classified into four levels by the International Society of Urological Pathology (ISUP)/World Health Organization (WHO) [12]. Based on the

assessment of nuclear prominence, Grade 1 is defined by inconspicuous/missing nuclei at $\times 400$ magnification. For grade 2, the nuclei are clearly visible at a magnification of $\times 400$ and for grade 3, the nuclei are visible at a magnification of $\times 100$. Finally, grade 4 tumors are highly polymorphic, with rhomboid and/or sarcomatoid differentiation [12].

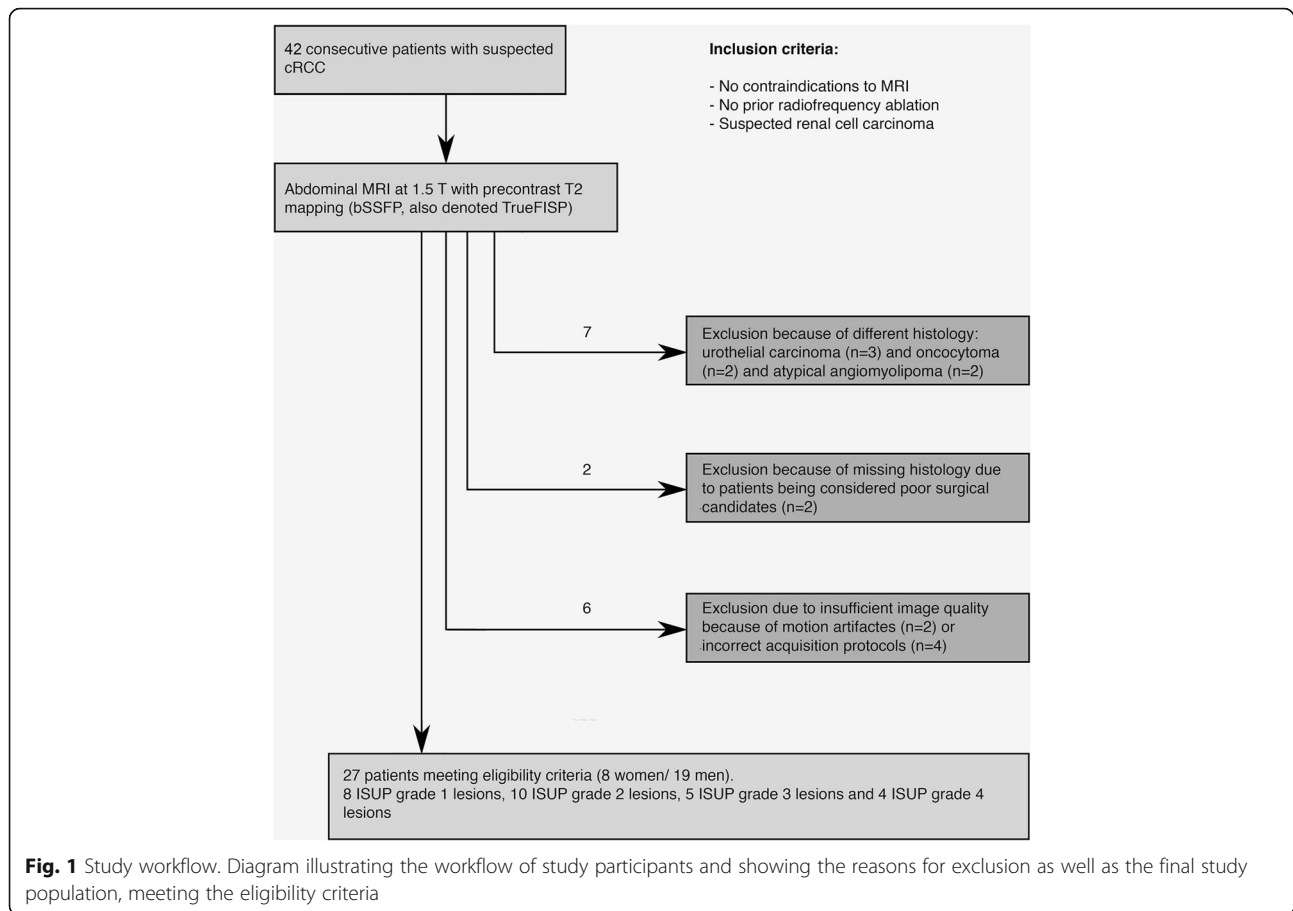
Statistical analysis

All statistical analysis was performed with the statistical software “R” (Version 3.2.2, R Development Core Team, 2015). Variables were averaged across measurements and expressed as mean \pm standard deviations in case of normal distribution and with median and interquartile range in absence of normal distribution. Students’ t-tests were used to evaluate the differences in mean values for continuous variables, while intergroup differences were tested for significance using the two-tailed Mann-Whitney-U test. Boxplots were created to show the distribution of the averaged quantitative T2 values among the different grades. To estimate the optimal cut-off T2 value for identifying a lower grade cRCC, a Receiver Operating Characteristic Curve (ROC) analysis was performed with exploratory selection of the optimal cut-off value. Sensitivity and specificity were calculated and based on values averaged over the two observers. Intraobserver and interobserver agreement were calculated using Bland Altman plots with limits of agreement and corresponding confidence intervals, whereby for the intraobserver agreement a graphical method for assessment of more than two readings was used [20]. In addition, the Coefficient of Variation (CoV) and the intraclass coefficient (ICC) were calculated. For the ICC, reliability was defined as excellent for values above 0.9, as good for values between 0.75 and 0.90, as moderate for 0.5–0.75 and as poor for values below 0.5 [21]. A p -value < 0.05 was considered to indicate a significant difference.

Results

The final study population consisted of 27 patients (19 men, 8 women, mean age, 61.3 ± 14.2 ; age range, 34–87 years) with histologically diagnosed cRCC. Figure 1 provides a study workflow and Table 2 gives an overview of the study characteristics. 14 lesions were in the left kidney and 13 lesions were located in the right kidney.

Histologic classification of patients revealed 8 ISUP grade 1 lesions, 10 ISUP grade 2 lesions, 5 ISUP grade 3 lesions, and 4 ISUP grade 4 lesions. The maximum cRCC diameter as determined in T2 HASTE images, using the longest tumor diameter in coronal sections, was between 1.4 cm and 17 cm (median of 4, interquartile range of 4.7). There was no difference in tumor size between men and women ($p = 0.21$). The



interval between MRI imaging and surgical removal was 25.1 ± 20.7 days.

T2 mapping results for different tumor grades

The distribution of native T2 relaxation times across different tumor grades can be seen in Fig. 2. Exemplary T2 maps of cRCC patients with different ISUP grades are shown in Fig. 3. T2 relaxation times were higher in lower grade cRCC compared to higher grade cRCC (132 ± 22 ms versus 97 ± 12 ms), with statistical analysis confirming a statistically significant difference ($p < 0.001$). We also looked at the distribution of T2 values in the tumor area based on a whole-tumor-approach, using density plots (refer to Additional file 2: Figure S2 and Additional file 3: Figure S3).

Average T2 values were $134 \text{ ms} \pm 20$ ms for ISUP grade 1, $128 \text{ ms} \pm 21$ ms for ISUP grade 2, $108 \text{ ms} \pm 19$ ms for ISUP grade 3 and $96 \text{ ms} \pm 6$ ms for ISUP grade 4 tumors. For the normal renal cortex and medulla, the average T2 values were 92 ± 16 and 85 ± 16 , respectively. There was no significant correlation between values for renal medulla, cortex and the glomerular filtration rate ($r = 0.21$, $p = 0.89$).

Diagnostic performance of T2 mapping

A ROC analysis was performed to determine the optimal T2 cut-off-value for the distinction of lower grade from higher grade cRCC. A cut-off-value of 110 ms could be identified to detect lower grade cRCC with a sensitivity of 83.3% (95% CI: 0.59–0.96) and a specificity of 88.9% (95% CI: 0.52–1.00) (refer to Table 3 for confusion matrix). However, four cases were wrongly diagnosed based on T2 mapping: Three lower grade cRCC were instead classified as higher grade cRCC based on their T2 values. Therefore, based on MRI, the severity of the case was overestimated. And one higher grade cRCC was wrongly classified as lower grade tumor. In this case, MRI underestimated the severity of the case.

Intraobserver and interobserver agreement

Regarding intraobserver assessment, the confidence intervals with a line of zero difference were 0 (95% CI: $-6.92 - 6.92$) for cRCC with a Coefficient of Variation (CoV) of 0.03, 0 (95% CI: $-6.74 - 6.74$) for the renal cortex with a CoV of 0.03 and 0 (95% CI: $-7.18 - 7.18$) for the medullary pyramids with a Coefficient of Variation (CoV) of 0.03 (refer to Fig. 4). For interobserver assessment, the mean differences between two observers

Table 2 Characteristics of the Study Population

Number of patients with cRCC (men, percentage of total (%))	27 (19, 70.4)
Mean age of patients with cRCC \pm SD ^a	61.3 \pm 14.2
Median diameters for cRCC (IQR ^b)	
ISUP grade 1 (IQR)	3.5 (1.13)
ISUP grade 2 (IQR)	3.95 (3.3)
ISUP grade 3 (IQR)	15.5 (3.8)
ISUP grade 4 (IQR)	5.6 (2.7)
Partial nephrectomy (number, %)	15, 55.6
Radical nephrectomy (number, %)	10, 37.0
Biopsy (number, %)	2, 7.4
Imaging Characteristics.	
Average normal renal parenchyma T2 values (ms) \pm SD	
Renal cortex	85 \pm 16
Renal medulla	92 \pm 16
Average T2 values for cRCC (ms) \pm SD (number, %)	
ISUP grade 1 \pm SD	134 \pm 20 (8, 29.6)
ISUP grade 2 \pm SD	128 \pm 21 (10, 37.0)
ISUP grade 3 \pm SD	108 \pm 19 (5, 18.5)
ISUP grade 4 \pm SD	96 \pm 6 (4, 14.8)

^aSD Standard deviation, ^bIQR Interquartile range

were 1.81 (95% CI: -10.24 - 13.87) for cRCC, -2.5 (95% CI: -14.34 - 9.34) for the renal cortex and -0.59 (95% CI: -13.17 - 11.98) for the medullary pyramids (refer to Fig. 5). Corresponding to this, there was an excellent interobserver agreement for the cRCC T2 values (ICC 0.97, 95% CI 0.94–0.99), the medullary T2 values (ICC 0.92, 95% CI 0.85–0.96), and the cortex T2 values (ICC 0.94, 95% CI 0.88–0.97).

Discussion

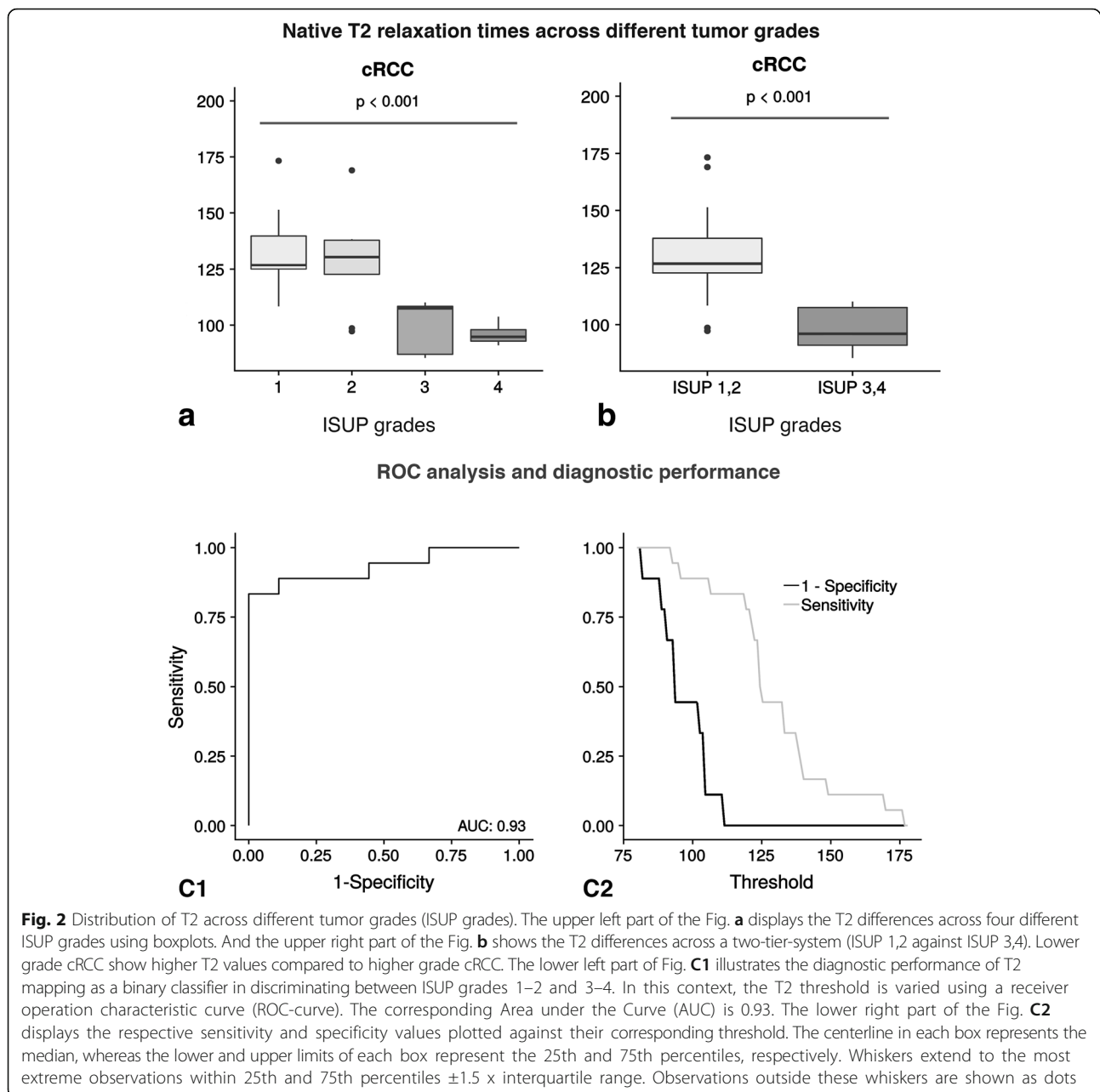
In this cross-sectional study, a quantitative T2 mapping technique (TrueFISP) was used for the differentiation of lower and higher grade cRCC. Lower grade cRCC (ISUP grades 1, 2) showed significantly higher T2 values compared to higher grade cRCC (ISUP grades 3, 4), supporting the potential of T2 mapping as a noninvasive marker of cRCC grade.

While conventional, qualitative T2 weighted imaging is subject to various limitations, such as the use of arbitrary signal intensity scales for T2 values with subsequent test-retest and interobserver variability, T2 mapping offers the potential for a standardized, reproducible assessment of tissue composition and water contents, e.g. facilitating the diagnosis of interstitial edema and extracellular space expansion [22, 23]. It is based on the acquisition of multiple T2-weighted images at different echo times (TE), with the signal of the various TEs being fitted to an exponential signal decay model, generating an estimate of quantitative T2

values [24]. Direct quantification of the T2 signal provides a benefit over T2-weighted imaging, minimizing dependency on user-defined parameters and subjective interpretation. Besides, differences between tissues might be detected more easily [7]. In the context of cardiac imaging, T2 mapping offers advantages over conventional T2 weighted imaging, for example in the detection of global myocardium changes in myocarditis or cardiac allograft rejection [25, 26]. For oncological imaging, T2 mapping was previously used for a range of different malignancies, such as colorectal carcinoma, breast and ovarian cancer, prostate carcinoma, glioblastoma and brain metastases [27–32]. Only a handful of prior studies focused on renal T2 mapping, e.g. showing the potential to evaluate the renal parenchyma after kidney transplantation and to improve the diagnosis/progression of polycystic kidney disease [11, 33]. Medullary T2 relaxation times were observed to be consistently longer compared to cortical T2 relaxation times, which is in accordance with the results of the present study [13]. To our knowledge, T2 mapping has so far not been examined in the context of cRCC.

Non-invasive cRCC grading would not only improve preoperative planning options, but also aid in prognosis assessment and prior patient information, for example by informing patients about the best individual therapy options. Furthermore, it may reduce the need for kidney mass biopsies. In addition, it might prevent cases of up-staging after partial nephrectomy in larger tumors, help identify patients who might be eligible for immunotherapy, and, finally, facilitate the selection of patients suitable for less invasive therapies [27], including minimally invasive procedures such as ablation, cryotherapy or even active surveillance. In addition to image-based grading of cRCC, image-based identification of different renal tumor subtypes such as urothelial carcinomas, oncocytomas, chromophobic RCC or lipid-poor angiomyolipomas would also be highly beneficial, because it could reduce the number of unnecessary surgical resections (9, 39). In the present study, however, the number of subtypes other than cRCC was too small to allow a valid evaluation (3 urothelial carcinomas, 2 oncocytomas, 2 atypical angiomyolipomas). Further studies are warranted to better assess the clinical feasibility of T2 mapping for the noninvasive assessment of cRCC, focusing on the ability to predict both tumor grade and subtype.

Regarding histology, cRCC consists of cells with clear cytoplasm and necrosis with often occurring cystic degeneration or hemorrhage [34]. Lower grade cRCC are predominantly characterized by cystic changes, which could serve as an explanation for the observed prolonged relaxation times. Necrosis, on the other hand, is particularly common in higher grade cRCC [6]. It does not only occur as macroscopic necrosis, but also as micronecrosis



below the spatial resolution of MRI [6, 35, 36]. In the present study, false negative results (lower grade cRCC with T2 values below 110 ms) could thus have resulted from including areas of (micro)necrosis within the ROI analysis [37, 38]. Decreased T2 relaxation times in higher grade tumors may be based on the presence of densely packed proliferating cells, interstitial reticulin deposition and/or irregular tumor vasculature [39, 40]. The false positive result in our study could have resulted from the inclusion of (micro)cystic components.

Although a considerable difference in the average T2 relaxation times between lower grade and higher grade

cRCC was observed in a two-tier-system, there was a significant overlap between the subgroups (ISUP 1,2 and ISUP 3,4) with no apparent difference. As a consequence, based on our data, it was not possible to differentiate between ISUP grade 1 and 2 or ISUP grade 3 and 4 tumors. However, the number of patients in the subgroups, especially regarding higher grade tumors, was very small and future studies with larger case numbers might help to assess the feasibility of T2 mapping in a four-tier-grading system, potentially allowing for/leading to T2 mapping value reference ranges with diagnostic utility. On route towards renal T2 mapping as a

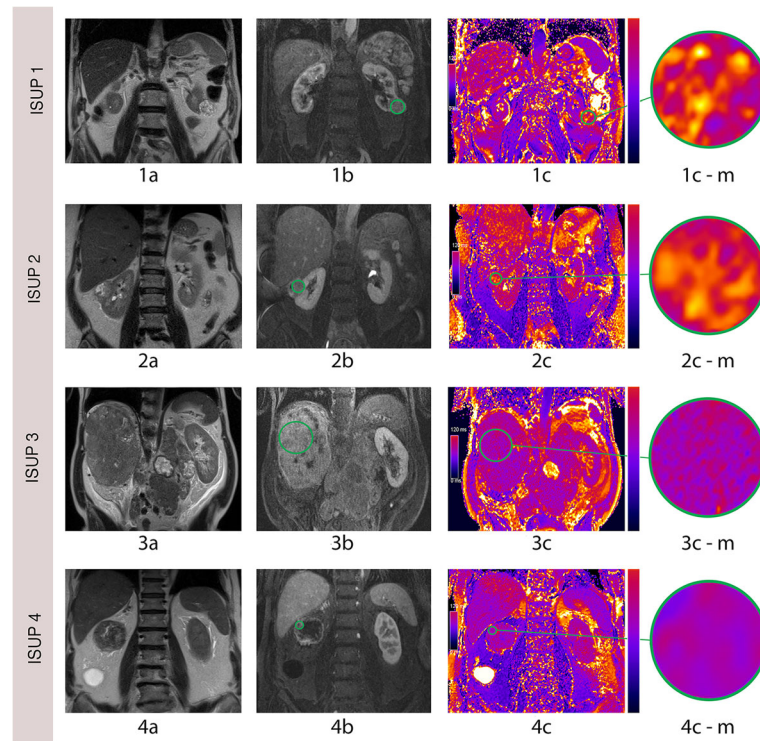


Fig. 3 Exemplary T2 mapping images of lower and higher grade cRCC. 1a, coronal T2 HASTE image of a 77-year-old man with a low grade (ISUP 1) cRCC of the left kidney. 1b, postcontrast T1 FLASH image. 1c, corresponding TrueFISP image, showing a high T2 signal. 2a, T2 HASTE image of a 57-year-old woman with a lower grade (ISUP 2) cRCC of the right kidney. 2b, postcontrast T1 FLASH image. 2c, corresponding TrueFISP image, also showing a high T2 signal (2d). 3a, coronal T2 HASTE image of a 62-year-old man with a higher grade (ISUP 3) cRCC of the right kidney. 3b, postcontrast T1 FLASH image. 3c, corresponding TrueFISP image, showing a low T2 signal. 4a, coronal T2 HASTE image of a 71-year-old man with a high grade (ISUP 4) cRCC of the right kidney. 4b, postcontrast T1 FLASH image. 4c, corresponding TrueFISP image, showing a low T2 signal. 1c-m1, 2c-m1, 3c-m1 and 4c-m1 are magnifications of 1c, 2c, 3c and 4c

potential additional biomarker, it will, furthermore, be necessary to validate T2 mapping against accepted reference measurements, such as nuclear medicine evaluations as well as histological findings [13].

In the context of future clinical applications, the use of T2 mapping might be a helpful addition to multiparametric imaging instead of being used exclusively. To this end, a novel T2-mapping-derived parameter could be integrated into a multiparametric MR imaging model. In the context of radiomics, it could also be included as a quantitative imaging feature, be converted into minable data and aid in the building of predictive models. It can

be expected, that multiparametric approaches will yield superior diagnostic performance, when compared to single imaging parameters alone. Therefore, in the future, multiparametric approaches may enable reliable, noninvasive grading of cRCC.

Regarding practicability, the T2 mapping approach chosen in the present study would be easy to implement in a clinical setting, as no complex mathematical modeling is required and the TrueFISP sequence is already commercially available on some MR scanners. Furthermore, it enables the acquisition of T2 maps during MRI scanning with a short scanning time. TrueFISP has been

Table 3 Confusion matrix for the calculation of diagnostic accuracy

MR native T2 mapping (index test)	Pathology (reference standard)		Total
	Confirmed lower grade cRCC	Confirmed higher grade cRCC	
Lower grade cRCC (ISUP grades 1, 2)	15	1	16
Higher grade cRCC (ISUP grade 3, 4)	3	8	11
Total	18	9	27

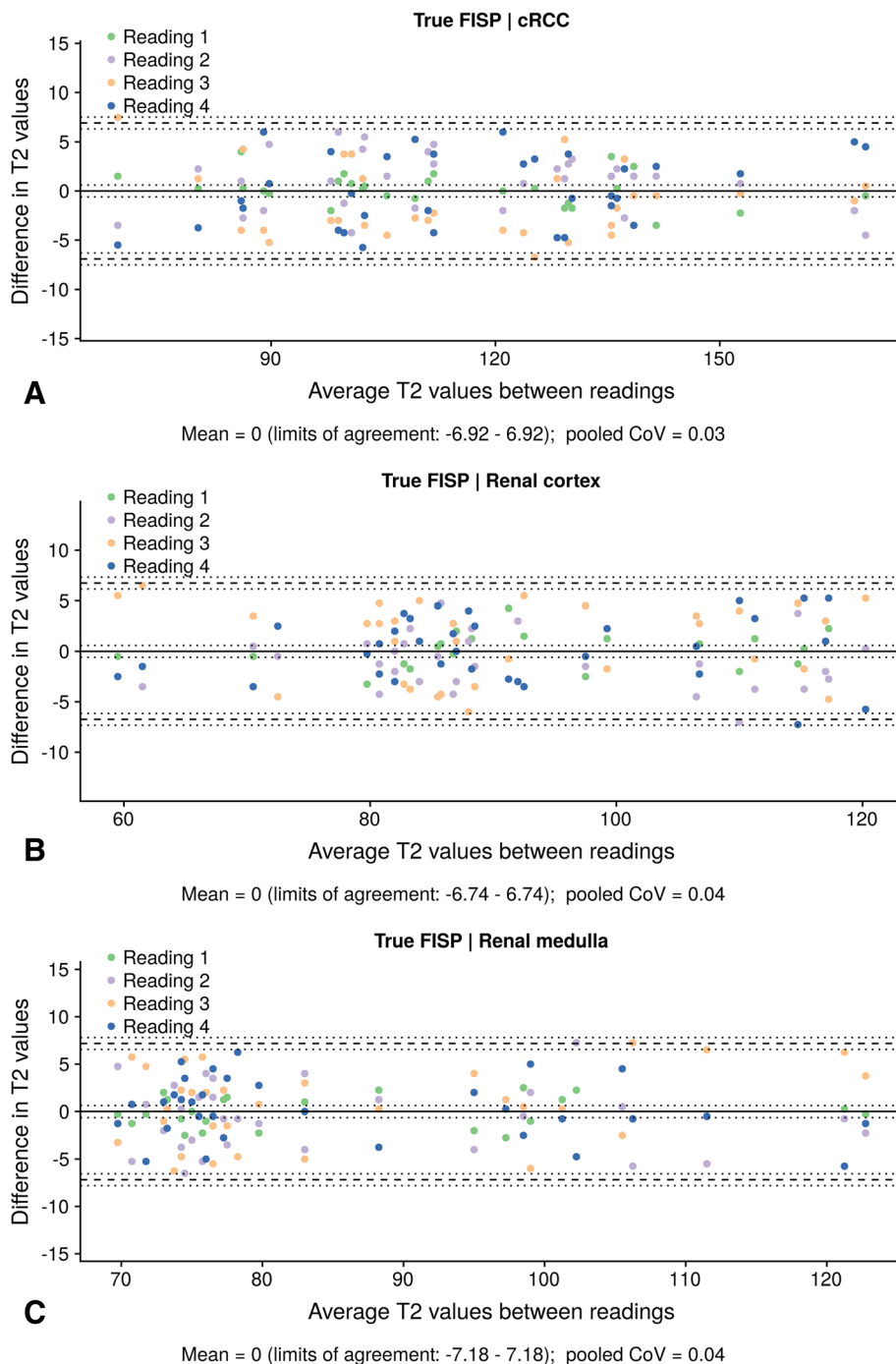
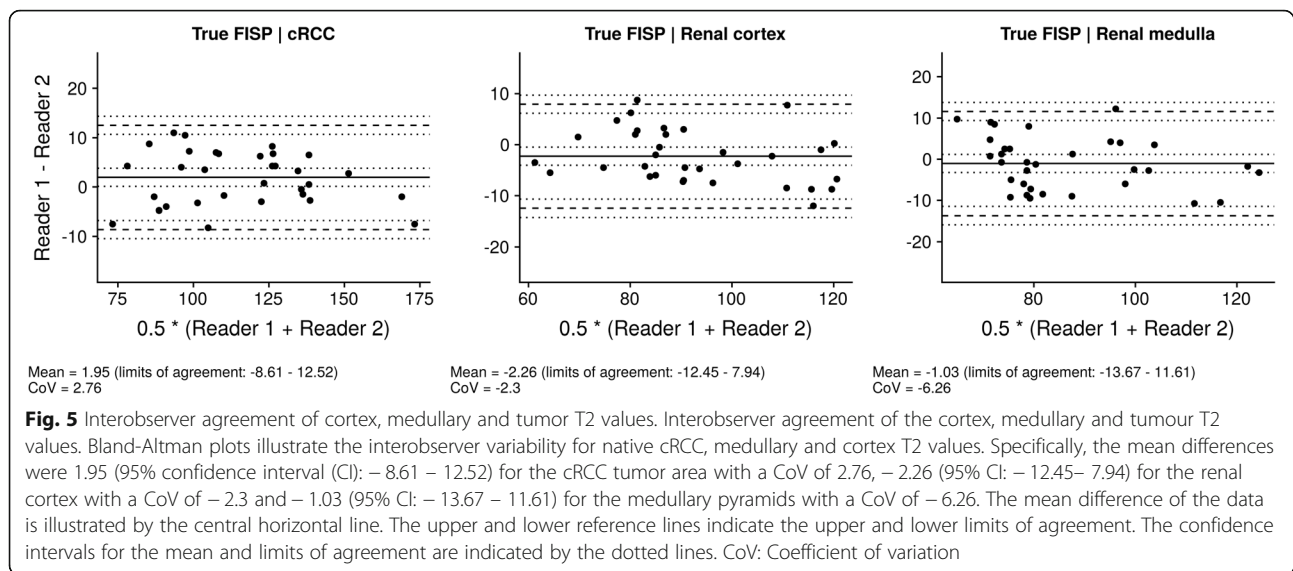


Fig. 4 Intraobserver agreement of cortex, medullary and tumor T2 values. Bland-Altman plots, showing agreement between four different readings for measurement of T2 values (**a**, tumor tissue; **b**, renal cortex; **c**, renal medulla). The upper and lower reference lines indicate the upper and lower limits of agreement (95% confidence intervals). The confidence intervals for the mean and limits of agreement are indicated by the dotted lines. CoV: Coefficient of variation

previously shown to be a robust method for T2 mapping, combining T2-magnetization preparation with steady-state free precession imaging and being sufficiently fast to be acquired in a single breathhold [41]. An advantage of T2-prepared single-shot TrueFISP is its high signal-to-

noise-ratio (SNR) and low sensitivity to breathing artifacts, which can be especially helpful in the assessment of cRCC, as kidney imaging is often limited by respiratory motion artefacts because of the location in the upper abdomen [7, 42]. Potential disadvantages of TrueFISP result from



the fact, that the number of acquired echoes is considerably lower compared to other techniques such as Multi Echo Spin Echo (MESE), providing only a limited number of data points along the T2 decay curve and thus potentially compromising accuracy and limiting its use to a narrower range of T2 species [43].

Due to the relatively long T2 relaxation times of the kidneys, ideally longer T2 preparation times with more than three weightings are used. While a repetition time of 1000 ms allows for time-efficient acquisition within a single breathhold, it does not ensure complete signal recovery. Therefore, the T2 maps in the present study are partly influenced by renal T1 signal and do not correspond to a pure T2 signal. To overcome this limitation in future studies, either the time of repetition can be increased (with a subsequent increase in scan time) or the flip angle can be reduced (with a decrease in SNR). However, within the scope of the present proof, we first aimed to investigate if a cardiac T2 mapping approach would be feasible for kidney imaging at all. Another limitation of this proof-of-concept study is, that it was based on a single-center design, only measuring T2 values at one time point prior to the intervention/surgery and including a small number of patients, especially with regard to higher grade cRCC. The small number of images was also an important limitation for assessment of intraobserver and interobserver agreement. In addition, the exclusion of other subtypes of renal masses brings about the risk of potential selection bias. Also, even though larger areas of necrosis were excluded, smaller necrotic regions may have been included in the ROI measurements and might have affected T2 measurements. Furthermore, the T2 relaxation time of the tumor was only measured in one representative coronal plane, not in the whole tumor. Besides, no

automatic motion or alignment correction was applied to correct for misregistrations between the different sequences. Therefore, slight misalignments cannot be completely excluded. Apart from that, even though patients were advised not to thirst and to drink water in the morning before the MRI, this was not explicitly controlled prior to the examination and patients were not instructed to drink a specific amount of water. Therefore, patients may have exhibited certain fluctuations in the hydration status, which could have affected T2 measurements in the renal parenchyma and potentially also in the tumor tissue. Finally, only one scanner from one vendor was used, therefore the results may not be generalizable to other institutions. Further investigations will be required to validate T2 mapping as a tool for cRCC assessment.

Conclusions

There was a significant difference in average T2 relaxation times between lower grade and higher grade cRCC, with lower grade cRCC showing significantly longer T2 relaxation times compared to higher grade cRCC. We therefore believe, that this technique holds potential for the future to noninvasively assess cRCC tumor grade in vivo and could provide a helpful addition to multiparametric imaging. However, studies with larger patient cohorts and a broader range of higher grade tumors are required to explore the utility of T2 mapping as a possible primary diagnostic MRI sequence for cRCC grading.

Additional files

Additional file 1: Figure S1. Visualization of circular 2D ROI placement for smaller tumors without and larger tumors with apparent necrosis

zones for ISUP grades 1 to 4. ROIs were first placed in a corresponding postcontrast image and then copied to the T2 map. (TIF 8355 kb)

Additional file 2: Figure S2. Segmentation of tumors (ISUP grades 1 to 4 from top to bottom, A-D) with creation of image masks (A2 through D2). A3 through D3 show the calculated percentage densities of the absolute T2 values. (TIF 2244 kb)

Additional file 3: Figure S3. The upper part of the figure illustrates the percentage density of T2 values for whole-tumor measurements of the four colour-coded ISUP grades (refer to the legend on the upper right side). For each tumor, the T2 maps were segmented and image masks were imported into the open access software 'R'. The lower part of the figure shows the colour-coded percentage density of T2 values for lower grade tumors (combined ISUP grades 1 and 2) and higher grade tumors (combined ISUP grades 3 and 4). (TIF 773 kb)

Abbreviations

CoV: Coefficient of Variation; cRCC: Clear-cell renal cell carcinoma; ICC: Intraclass correlation coefficient; ISUP: International Society of Urological Pathology; MRI: Magnetic resonance imaging; RCC: Renal cell carcinoma; ROC: Receiver Operating Characteristic Curve; ROI: Region of interest; SNR: Signal-to-noise-ratio; TE: Echo time; WHO: World Health Organization

Acknowledgements

MRM is grateful for support from the Deutsche Forschungsgemeinschaft (DFG, SFB 1340/1 2018, 5943/31/41/91). LCA and BR are grateful for their participation in the BIH Charité - (Junior) Clinician Scientist Program funded by the Charité - Universitätsmedizin Berlin and the Berlin Institute of Health. JB is participant in the BIH - Twinning Grant Program funded by the Charité - Universitätsmedizin Berlin and the Berlin Institute of Health.

Authors' contributions

MRM and LCA conceived of the present idea. MRM supervised the project. LCA and KB acquired, analyzed and interpreted the patient data. LCA was a major contributor in writing the manuscript. BH, MRM, JB, PJ, UF, KB and GE gave technical support and conceptual advice. All authors read and revised the manuscript critically, approving the final manuscript.

Funding

BH has received research grants for the Department of Radiology, Charité – Universitätsmedizin Berlin from various technical and scientific companies, including: 1. Abbott, 2. Actelion Pharmaceuticals, 3. Bayer Schering Pharma, 4. Bayer Vital, 5. BRACCO Group, 6. Bristol-Myers Squibb, 7. Charite research organisation GmbH, 8. Deutsche Krebshilfe, 9. Dt. Stiftung für Herzforschung, 10. Essex Pharma, 11. EU Programmes, 12. Fibrex Medical Inc., 13. Focused Ultrasound Surgery Foundation, 14. Fraunhofer Gesellschaft, 15. Guerbet, 16. INC Research, 17. InSightec Ud., 18. IPSEN Pharma, 19. Kendle MorphoSys AG, 20. Lilly GmbH, 21. Lundbeck GmbH, 22. MeVis Medical Solutions AG, 23. Nexus Oncology, 24. Novartis, 25. Parexel Clinical Research Organisation Service, 26. Perceptiv, 27. Pfizer GmbH, 28. Philipps, 29. SanofiAventis S. A, 30. Siemens, 31. Spectranetics GmbH, 32. Terumo Medical Corporation, 33. TNS Healthcare GmbH, 34. Toshiba, 35. UCB Pharma, 36. Wyeth Pharma, 37. Zukunftsfond Berlin (TSB), 38. Amgen, 39. AO Foundation, 40. BARD, 41. BBraun, 42. Boehringer Ingelheimer, 43. Brainsgate, 44. PPD (Clinical Research Organisation), 45. CELLACT Pharma, 46. Celgene, 47. Celonova BioSciences, 48. Covance, 49. Deviees, Ine. USA, 50. Ganymed, 51. Gilead Sciences, 52. Glaxo Smith Kline, 53. ICON (Clinical Research Organisation), 54. Jansen, 55. LUX Bioeiences, 56. MedPass, 57. Merek, 58. Mologen, 59. Nuvisan, 60. Pluristem, 61. Quintiles, 62. Roehle, 63. Sehumaeher GmbH (Sponsoring eines Workshops), 64. Seattle Genetics, 65. Symphogen, 66. TauRx Therapeutics Ud., 67. Accovion, 68. AIO: Arbeitsgemeinschaft Internistische Onkologie, 69. ASR Advanced sleep research, 70. Astellas, 71. Theradex, 72. Galena Bio-pharma, 73. Chiltern, 74. PRAint, 75. Inspiremd, 76. Medronic, 77. Respicardia, 78. Silena Therapeutics, 79. Spectrum Pharmaceuticals, 80. St. Jude., 81. TEVA, 82. Theorem, 83. Abbvie, 84. Aesculap, 85. Biotronik, 86. Inventivhealth, 87. ISA Therapeutics, 88. LYSARC, 89. MSD, 90. novocure, 91. Ockham oncology, 92. Premier-research, 93. Psi-cro, 94. Tetec-ag, 94. Tetec-ag, 95. Winicker-norimed, 96. Achaogen Inc., 97. ADIR, 98. AstraZeneca AB, 99. Demira Inc., 100.Euroscreen S.A., 101. Galmed Research and Development Ltd., 102. GETNE, 103. Guidant Europe NV, 104. Holaira Inc., 105. Immunomedics Inc., 106. Innate Pharma, 107. Isis Pharmaceuticals Inc., 108. Kantar Health GmbH,

109. MedImmune Inc., 110. Medpace Germany GmbH (CRO), 111. Merrimack Pharmaceuticals Inc., 112. Millenium Pharmaceuticals Inc., 113. Orion Corporation Orion Pharma, 114. Pharmacyclis Inc., 115. PIQR Therapeutics Ltd., 116. Pulmonx International SárI, 117. Servier (CRO), 118. SGS Life Science Services (CRO), 119. Treshold Pharmaceuticals Inc. MRM is funded by the Deutsche Forschungsgemeinschaft (DFG, SFB 1340/1 2018, 5943/31/41/91). LCA and BR are participants in the BIH Charité - Junior Clinician Scientist Program funded by the Charité - Universitätsmedizin Berlin and the Berlin Institute of Health. JB is participant in the BIH - Twinning Grant Program funded by the Charité - Universitätsmedizin Berlin and the Berlin Institute of Health.

Availability of data and materials

The datasets used and/or analysed during the current study are available from the corresponding author on reasonable request.

Ethics approval and consent to participate

This cross-sectional study was approved by the Institutional Review Board ("Ethikkommission der Charité").

Consent for publication

Yes.

Competing interests

The authors declare that they have no competing interests.

Author details

¹Department of Radiology, Charité, Charitéplatz 1, 10117 Berlin, Germany. ²Department of Radiology, Charité, Hindenburgdamm 30, 12203 Berlin, Germany. ³Department of Pathology, Charité, Charitéplatz 1, 10117 Berlin, Germany. ⁴Department of Urology, Charité, Charitéplatz 1, 10117 Berlin, Germany.

Received: 14 January 2019 Accepted: 27 May 2019

Published online: 07 June 2019

References

1. Ferlay J, Steliarova-Foucher E, Lortet-Tieulent J, Rosso S, Coebergh JW, Comber H, Forman D, Bray F. Cancer incidence and mortality patterns in Europe: estimates for 40 countries in 2012. *Eur J Cancer*. 2013;49(6):1374–403.
2. Siegel RL, Miller KD, Jemal A. Cancer statistics, 2018. *CA Cancer J Clin*. 2018; 68(1):7–30.
3. Chevillet JC, Lohse CM, Zincke H, Weaver AL, Blute ML. Comparisons of outcome and prognostic features among histologic subtypes of renal cell carcinoma. *Am J Surg Pathol*. 2003;27(5):612–24.
4. Motzer RJ, Bacik J, Mariani T, Russo P, Mazumdar M, Reuter V. Treatment outcome and survival associated with metastatic renal cell carcinoma of non-clear-cell histology. *J Clin Oncol*. 2002;20(9):2376–81.
5. Jewett MA, Mattar K, Basiuk J, Morash CG, Pautler SE, Siemens DR, Tanguay S, Rendon RA, Gleave ME, Drachenberg DE, et al. Active surveillance of small renal masses: progression patterns of early stage kidney cancer. *Eur Urol*. 2011;60(1):39–44.
6. Cornelis F, Tricaud E, Lasserre AS, Petitpierre F, Bernhard JC, Le Bras Y, Yacoub M, Bouzgarrou M, Ravaud A, Grenier N. Multiparametric magnetic resonance imaging for the differentiation of low and high grade clear cell renal carcinoma. *Eur Radiol*. 2015;25(1):24–31.
7. Giri S, Chung YC, Merchant A, Mihai G, Rajagopalan S, Raman SV, Simonetti OP. T2 quantification for improved detection of myocardial edema. *J Cardiovasc Magn Reson*. 2009;11:56.
8. Abdel-Aty H, Schulz-Menger J. Cardiovascular magnetic resonance T2-weighted imaging of myocardial edema in acute myocardial infarction. *Recent Pat Cardiovasc Drug Discov*. 2007;2(1):63–8.
9. Kramer CM, Chandrashekar Y, Narula J. T1 mapping by CMR in cardiomyopathy: a noninvasive myocardial biopsy? *JACC Cardiovasc Imaging*. 2013;6(4):532–4.
10. Selby NM, Blankestijn PJ, Boor P, Combe C, Eckardt KU, Eikefjord E, Garcia-Fernandez N, Golay X, Gordon I, Grenier N, et al. Magnetic resonance imaging biomarkers for chronic kidney disease: a position paper from the European Cooperation in Science and Technology action PARENCHIMA. *Nephrol Dial Transplant*. 2018;33(suppl_2):ii4–ii14.
11. Franke M, Baessler B, Vechtel J, Dafinger C, Hohne M, Borgal L, Gobel H, Koerber F, Maintz D, Benzinger T, et al. Magnetic resonance T2 mapping and

- diffusion-weighted imaging for early detection of cystogenesis and response to therapy in a mouse model of polycystic kidney disease. *Kidney Int.* 2017; 92(6):1544–54.
12. Luetkens JA, Klein S, Traber F, Schmeel FC, Sprinkart AM, Kuetting DLR, Block W, Uschner FE, Schierwagen R, Hittatiya K, et al. Quantification of liver fibrosis at T1 and T2 mapping with extracellular volume fraction MRI: preclinical results. *Radiology.* 2018;288(3):748–54.
 13. Wolf M, de Boer A, Sharma K, Boor P, Leiner T, Sunder-Plassmann G, Moser E, Caroli A, Jerome NP. Magnetic resonance imaging T1- and T2-mapping to assess renal structure and function: a systematic review and statement paper. *Nephrol Dial Transplant.* 2018;33(suppl_2):ii41–50.
 14. Kitis O, Altay H, Calli C, Yuntun N, Akalin T, Yurtseven T. Minimum apparent diffusion coefficients in the evaluation of brain tumors. *Eur J Radiol.* 2005; 55(3):393–400.
 15. Al Nazer M, Mourad WA. Successful grading of renal-cell carcinoma in fine-needle aspirates. *Diagn Cytopathol.* 2000;22(4):223–6.
 16. Brittain JH, Hu BS, Wright GA, Meyer CH, Macovski A, Nishimura DG. Coronary angiography with magnetization-prepared T2 contrast. *Magn Reson Med.* 1995;33(5):689–96.
 17. Shea SM, Deshpande VS, Chung YC, Li D. Three-dimensional true-FISP imaging of the coronary arteries: improved contrast with T2-preparation. *J Magn Reson Imaging.* 2002;15(5):597–602.
 18. Pallwein-Pretner L, Flory D, Rotter CR, Pogner K, Syre G, Fellner C, Fauscher F, Aigner F, Krause FS, Fellner F. Assessment and characterisation of common renal masses with CT and MRI. *Insights Imaging.* 2011;2(5):543–56.
 19. Oto A, Herts BR, Remer EM, Novick AC. Inferior vena cava tumor thrombus in renal cell carcinoma: staging by MR imaging and impact on surgical treatment. *AJR Am J Roentgenol.* 1998;171(6):1619–24.
 20. Jones M, Dobson A, O'Brian S. A graphical method for assessing agreement with the mean between multiple observers using continuous measures. *Int J Epidemiol.* 2011;40(5):1308–13.
 21. Koo TK, Li MY. A guideline of selecting and reporting Intraclass correlation coefficients for reliability research. *J Chiropr Med.* 2016;15(2):155–63.
 22. Vermes E, Pantaleon C, Auvert A, Cazeneuve N, Mchet MC, Delhommeais A, Bourguignon T, Aupart M, Brunereau L. Cardiovascular magnetic resonance in heart transplant patients: diagnostic value of quantitative tissue markers: T2 mapping and extracellular volume fraction, for acute rejection diagnosis. *J Cardiovasc Magn Reson.* 2018;20(1):59.
 23. Messroghli DR, Plein S, Higgins DM, Walters K, Jones TR, Ridgway JP, Sivanathan MU. Human myocardium: single-breath-hold MR T1 mapping with high spatial resolution—reproducibility study. *Radiology.* 2006;238(3):1004–12.
 24. Foltz WD, Chopra S, Chung P, Bayley A, Catton C, Jaffray D, Wright GA, Haider MA, Menard C. Clinical prostate T2 quantification using magnetization-prepared spiral imaging. *Magn Reson Med.* 2010;64(4):1155–61.
 25. Butler CR, Thompson R, Haykowsky M, Toma M, Paterson I. Cardiovascular magnetic resonance in the diagnosis of acute heart transplant rejection: a review. *J Cardiovasc Magn Reson.* 2009;11:7.
 26. Abdel-Aty H, Boye P, Zagrosek A, Wassmuth R, Kumar A, Messroghli D, Bock P, Dietz R, Friedrich MG, Schulz-Menger J. Diagnostic performance of cardiovascular magnetic resonance in patients with suspected acute myocarditis: comparison of different approaches. *J Am Coll Cardiol.* 2005;45(11):1815–22.
 27. Yamada I, Yoshino N, Hikishima K, Miyasaka N, Yamauchi S, Uetake H, Yasuno M, Saida Y, Tateishi U, Kobayashi D, et al. Colorectal carcinoma: ex vivo evaluation using 3-T high-spatial-resolution quantitative T2 mapping and its correlation with histopathologic findings. *Magn Reson Imaging.* 2017;38:174–81.
 28. Liu L, Yin B, Shek K, Geng D, Lu Y, Wen J, Kuai X, Peng W. Role of quantitative analysis of T2 relaxation time in differentiating benign from malignant breast lesions. *J Int Med Res.* 2018;46(5):1928–35.
 29. Chatterjee A, Devaraj A, Mathew M, et al. Performance of T2 Maps in the Detection of Prostate Cancer. *Acad Radiol.* 2019;26(1):15–21.
 30. Carter JS, Koopmeiners JS, Kuehn-Hajder JE, Metzger GJ, Lakkadi N, Downs LS Jr, Bolan PJ. Quantitative multiparametric MRI of ovarian cancer. *J Magn Reson Imaging.* 2013;38(6):1501–9.
 31. Hattingen E, Jurcoane A, Daneshvar K, Pilatus U, Mittelbronn M, Steinbach JP, Bahr O. Quantitative T2 mapping of recurrent glioblastoma under bevacizumab improves monitoring for non-enhancing tumor progression and predicts overall survival. *Neuro-Oncology.* 2013;15(10):1395–404.
 32. Nakai K, Nawashiro H, Shima K, Kaji T. An analysis of T2 mapping on brain tumors. *Acta Neurochir Suppl.* 2013;118:195–9.
 33. Hueper K, Hensen B, Gutberlet M, Chen R, Hartung D, Barmmeyer A, Meier M, Li W, Jang MS, Mengel M, et al. Kidney transplantation: multiparametric functional magnetic resonance imaging for assessment of renal allograft pathophysiology in mice. *Investig Radiol.* 2016;51(1):58–65.
 34. Campbell N, Rosenkrantz AB, Pedrosa I. MRI phenotype in renal cancer: is it clinically relevant? *Top Magn Reson Imaging.* 2014;23(2):95–115.
 35. Delahunt B, McKenney JK, Lohse CM, Leibovich BC, Thompson RH, Boorjian SA, Chevillet JC. A novel grading system for clear cell renal cell carcinoma incorporating tumor necrosis. *Am J Surg Pathol.* 2013;37(3):311–22.
 36. Klatt T, Said JW, de Martino M, Larochelle J, Shuch B, Rao JY, Thomas GV, Kabbinnar FF, Belldegrun AS, Pantuck AJ. Presence of tumor necrosis is not a significant predictor of survival in clear cell renal cell carcinoma: higher prognostic accuracy of extent based rather than presence/absence classification. *J Urol.* 2009;181(4):1558–64 discussion 1563–1554.
 37. Biasioli L, Lindsay AC, Chai JT, Choudhury RP, Robson MD. In-vivo quantitative T2 mapping of carotid arteries in atherosclerotic patients: segmentation and T2 measurement of plaque components. *J Cardiovasc Magn Reson.* 2013;15:69.
 38. Merchant TE, Thelissen GR, de Graaf PW, Nieuwenhuizen CW, Kievit HC, Den Otter W. Application of a mixed imaging sequence for MR imaging characterization of human breast disease. *Acta Radiol.* 1993;34(4):356–61.
 39. Farrar CT, Kamoun WS, Ley CD, Kim YR, Catana C, Kwon SJ, Rosen BR, Jain RK, Sorensen AG. Sensitivity of MRI tumor biomarkers to VEGFR inhibitor therapy in an orthotopic mouse glioma model. *PLoS One.* 2011;6(3):e17228.
 40. Oh J, Cha S, Aiken AH, Han ET, Crane JC, Stainsby JA, Wright GA, Dillon WP, Nelson SJ. Quantitative apparent diffusion coefficients and T2 relaxation times in characterizing contrast enhancing brain tumors and regions of peritumoral edema. *J Magn Reson Imaging.* 2005;21(6):701–8.
 41. Huang TY, Liu YJ, Stemmer A, Poncet BP. T2 measurement of the human myocardium using a T2-prepared transient-state TrueFISP sequence. *Magn Reson Med.* 2007;57(5):960–6.
 42. Pedrosa I, Alsop DC, Rofsky NM. Magnetic resonance imaging as a biomarker in renal cell carcinoma. *Cancer.* 2009;115(10 Suppl):2334–45.
 43. Baessler B, Schaarschmidt F, Stehning C, Schnackenburg B, Maintz D, Bunc AC. Cardiac T2-mapping using a fast gradient echo spin echo sequence - first in vitro and in vivo experience. *J Cardiovasc Magn Reson.* 2015;17:67.

Publisher's Note

Springer Nature remains neutral with regard to jurisdictional claims in published maps and institutional affiliations.

Ready to submit your research? Choose BMC and benefit from:

- fast, convenient online submission
- thorough peer review by experienced researchers in your field
- rapid publication on acceptance
- support for research data, including large and complex data types
- gold Open Access which fosters wider collaboration and increased citations
- maximum visibility for your research: over 100M website views per year

At BMC, research is always in progress.

Learn more biomedcentral.com/submissions

